# Fabrication of Quantum Dot Microarrays Using Electron Beam Lithography for Applications in Analyte Sensing and Cellular Dynamics

Raghavendra Palankar,[§,*] Nikolay Medvedev,[§] Alena Rong, and Mihaela Delcea[*]

Nanostructure Group, ZIK HIKE - Center for Innovation Competence, Humoral Immune Reactions in Cardiovascular Diseases, Ernst-Moritz-Arndt-Universität Greifswald, 17489 Greifswald, Germany. [§]These authors contributed equally to this work.

ABSTRACT Quantum dot (QD) based micro-/nanopatterned arrays are of broad interest in applications ranging from electronics, photonics, to sensor devices for biomedical purposes. Here, we report on a rapid, physico-chemically mild approach to generate high fidelity micropattern arrays of prefunctionalized water-soluble quantum dots using electron beam lithography. We show that such patterns retain their fluorescence and bioaffinity upon electron beam lithography and, based on the streptavidin—biotin interaction, allow for detection of proteins, colloidal gold nanoparticles and magnetic microparticles. Furthermore, we demonstrate the applicability of QD based microarray patterns differing in their shape (circles, squares,

grid-like), size (from 1 to 10 μm) and pitch distance to study the adhesion, spreading and migration of human blood derived neutrophils. Using live cell confocal fluorescence microscopy, we show that pattern geometry and pitch distance influence the adhesion, spreading and migratory behavior of neutrophils. Research reported in this work paves the way for producing QD microarrays with multiplexed functionalities relevant for applications in analyte sensing and cellular dynamics.
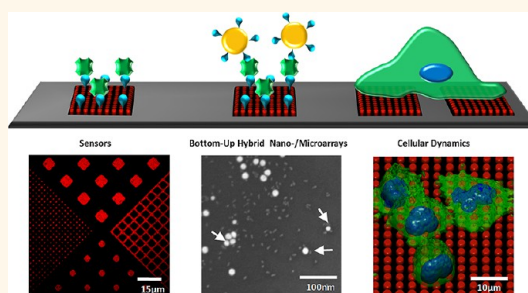
KEYWORDS: electron beam lithography · quantum dots · micropattern arrays · neutrophils · live cell imaging

Hybrid micro-/nanoarrays are of significant interest for regenerative medicine,[1−3] biosensing,[4,5] cell-based assays for high-throughput screening[6] and scaffolds for tissue and cell engineering.[7,8] Nanofabrication technologies enable the fabrication of micro-/nanoarrays with defined properties (*e.g.*, shape, size and pitch distance) offer unlimited possibilities to develop efficient sensors for monitoring and quantifying analytes and to probe the dynamics of cellular processes (*e.g.*, adhesion, spreading, migration, division and differentiation).

Recently, there has been a great interest to pattern surfaces with Quantum Dots (QDs) and QD bioconjugates due to their tunable optical and electrical properties.[9] Patterned QD surfaces have been widely used in the field of photonics[10] and hybrid organic/inorganic solar cells.[11] During the past few years, several strategies have been developed to generate nano- and micropatterned structures of QDs and QD bioconjugates with controlled size and shape using particle lithography,[12,13] dip-pen nanolithography,[14,15] click microcontact printing[16] and electron beam lithography.[17−21]

Since there is a growing interest in generating high quality robust arrays of QDs for biomedical applications, water-soluble QDs[22,23] are being developed. Different methods to prepare water-soluble QDs involving the replacement of hydrophobic ligands by water-soluble bifunctional molecules have been established.[24−26] Water-soluble QD micro-/nanoarrays are excellent candidates to develop biosensor devices since they display temperature and pH responsive fluorescence behavior.[27] Khalid *et al.* immobilized *via* dithiol linker Cd QDs on a gold electrode which was additionally modified with FePt particles. Such a light-addressable sensor was used to detect hydrogen peroxide *via* catalytic degradation

at the surface of FePt NPs and charge transfer from the electrode *via* CdS QDs.[28]

Alternatively to patterns made of gold[29−31] and titanium nanoparticles,[32] patterns based on QDs and QDs and their bioconjugates offer substantial advantage due to their luminescent properties.

A variety of techniques have been developed to organize colloidal particles into highly ordered structures. For instance, wrinkle-assisted assembly allows the ordering of particles into highly regular wrinkles formed upon exposure of elastomeric materials with hard top coatings to compressive strains.[33,34] Such systems are excellent candidates for designing high-efficiency sensors. Alternatively, we have used Electron Beam Lithography (EBL) to create line patterns by specific binding of streptavidin functionalized magnetic microbeads to QD-biotin.

QD layers on cell culture dishes have been previously used to study *in vitro* invasively and noninvasively cancer cell lines and cell signaling events involved in cell migration.[35,36]

EBL offers possibilities to fabricate arrays of QDs in geometrically defined micro/nano patterns which can further aid to investigate the complexities of immune defense mechanisms that involve cellular motility and navigation toward pathogens. One of the most important subsets of blood cells that show rapid response and migration toward inflammation and pathogen invasion are the neutrophils. As an integral part of the immune system, neutrophils are the first line of defense and are responsible for elimination of microbes by phagocytosis. They produce reactive oxygen species, cationic antimicrobial peptides, proteolytic enzymes, metal chelator proteins and neutrophil extracellular traps (NETs). In addition, neutrophiles participate in immune cell cross-talk and play significant roles in certain malignant cancer tumor growth and in autoimmune diseases.[37,38]

This intricacy in the biological interaction and function of neutrophils requires innovative experimental platforms to further elucidate the role of neutrophils in immune response. Initiatives in this direction especially from the field of microfabrication techniques have provided important observations related to neutrophil rolling under flow conditions in microfluidic channels,[39,40] control of neutrophil spreading on micropatterned protein surfaces[41] and their motility on chemically and geometrically defined micropatterns.[42−44]

Here we describe a rapid, physico-chemically mild approach to generate high fidelity micropattern arrays of prefunctionalized water-soluble QDs by direct writing using EBL which enables homogeneous and highly accurate arrays structures of less than 50 nm dimensions.[45] Because of the possible loss in QD fluorescence and also in their biofunctionality upon
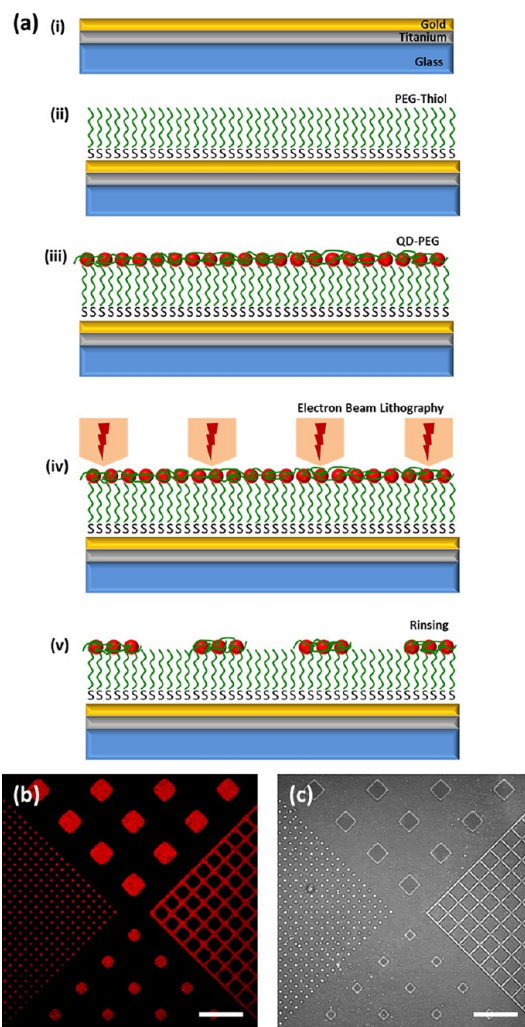
Figure 1. EBL based patterning of quantum dots: (a) schematics of steps involved in EBL based micropatterning of QD-PEG. (i) glass coverslip coated with gold on a layer of titanium is (ii) functionalized with PEG-thiol onto which (iii) another layer of QD-PEG suspension is spin coated and exposed to (iv) electron beam creating defined patterns while (v) non-cross-linked QDs are washed away by rinsing with deionized water; (b and c) CLSM fluorescence and DIC images of EBL micropatterns of QD-PEG. Scale bars correspond to 20 μm.

exposure to the electron beam during patterning process, we investigate the influence of the electron beam dosage on these properties. We show that QD micropatterns retain their fluorescence and bioaffinity upon EBL and based on the streptavidin−biotin interaction, allowing for the specific detection of proteins, colloidal gold nanoparticles and magnetic microparticles. In addition, we investigate the adhesion, spreading and migration of human blood derived neutrophils on polyethylene glycol conjugated QDs (QD-PEG) embedded in a matrix of PEG-ylated poly-L-lysine (PLL-PEG) of different shape (circles, squares, grid-like), size (ranging from 1 to 10 μm) and pitch distances. To the best of our knowledge, this is the first study on the use of prefunctionalized water-soluble QD micropattern arrays to detect biomolecular analytes based on
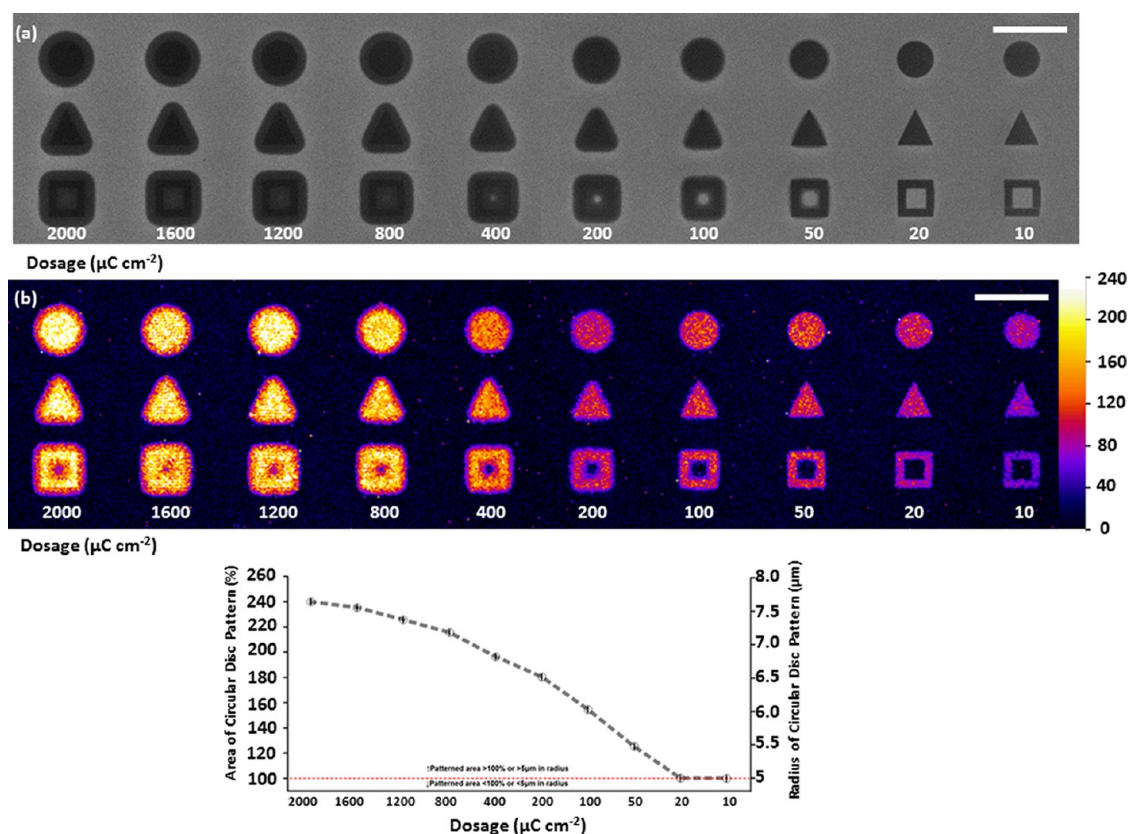
Figure 2. Characterization of the effect of electron beam dosage on the fidelity of QD micropatterns: (a) SEM image of QD-PEG micropatterns obtained by varying the dosage of the electron beam for the patterning process. (b) LUT of fluorescence intensities of the CLSM fluorescence image of electron beam dosage on QD-PEG micropatterns. (c) The effect of electron beam dosage on the patterned area and its radius on circular disc shaped patterns upon EBL. Scale bars correspond to 20 μm.

specific binding and also to investigate the cellular dynamics of neutrophils.

RESULTS AND DISCUSSION

EBL Micropatterning of Water-Soluble Quantum Dots and the Effect of Electron Beam Dosage on Micropattern Fidelity. Previous studies have shown that QDs soluble in organic solvents can be used to create patterns using EBL.[19,20,46,47] However, micropatterns of QDs solubilized in organic solvents have several limitations as they cannot be readily functionalized upon fabrication of the micropatterns. To circumvent these issues, Rotello and co-workers used trioctylphosphine oxide functionalized QDs (TOPO-QDs) that were postfunctionalized with cationic ligands to electrostatically bind tdTomato fluorescent protein after EBL.[20] In our work, we first tested the feasibility of prefunctionalized water-soluble QD-PEG to create micropatterns of various shapes and dimensions using EBL.

The fabrication of the micropatterns with water-soluble QDs is schematically represented in Figure 1a. Briefly, a glass coverslip was sputter coated with titanium and gold layers, respectively (step i), on top of which a self-assembled monolayer (SAM) of PEG-thiol was grafted (step ii). We used PEG because it is widely used as electron beam resist, available with a

wide range of chemical modifications (e.g., PLL, alkanethiols or silanes) and biologically inert and immunogenically neutral.[48,49] A mixture of QD-PEG and PLL-PEG was then spin coated to create a film (step iii) on the SAM of PEG-thiol. Ellipsometric measurements of the spin coated PLL-PEG:QD film on top of PEG-thiol SAM before EBL showed an average thickness of approximatively 90 nm. Upon exposure to EBL (step iv), QD-PEG was cross-linked and the non-cross-linked QD-PEG was removed by rinsing with deionized water revealing the micropatterns (step v). Confocal laser scanning microscopy (CLSM) and differential interference contrast (DIC) images of an array of QD-PEG micropatterns of precise geometries formed by EBL at accelerating voltage of 5 kV and electron beam dosage of 20 μC cm^{-2} are shown in Figure 1b,c. It is important to notice in Figure 1b the sharp boundaries of the micropatterns and the absence of background fluorescence from QDs beyond the electron beam exposed area.

Previous studies on electron beam mediated cross-linking of organic films have shown that the degree of cross-linking depends on the electron beam dosage.[50−52] To characterize the effect of electron beam dosage on micropattern fidelity and also its effect on fluorescence intensity of the QDs in the
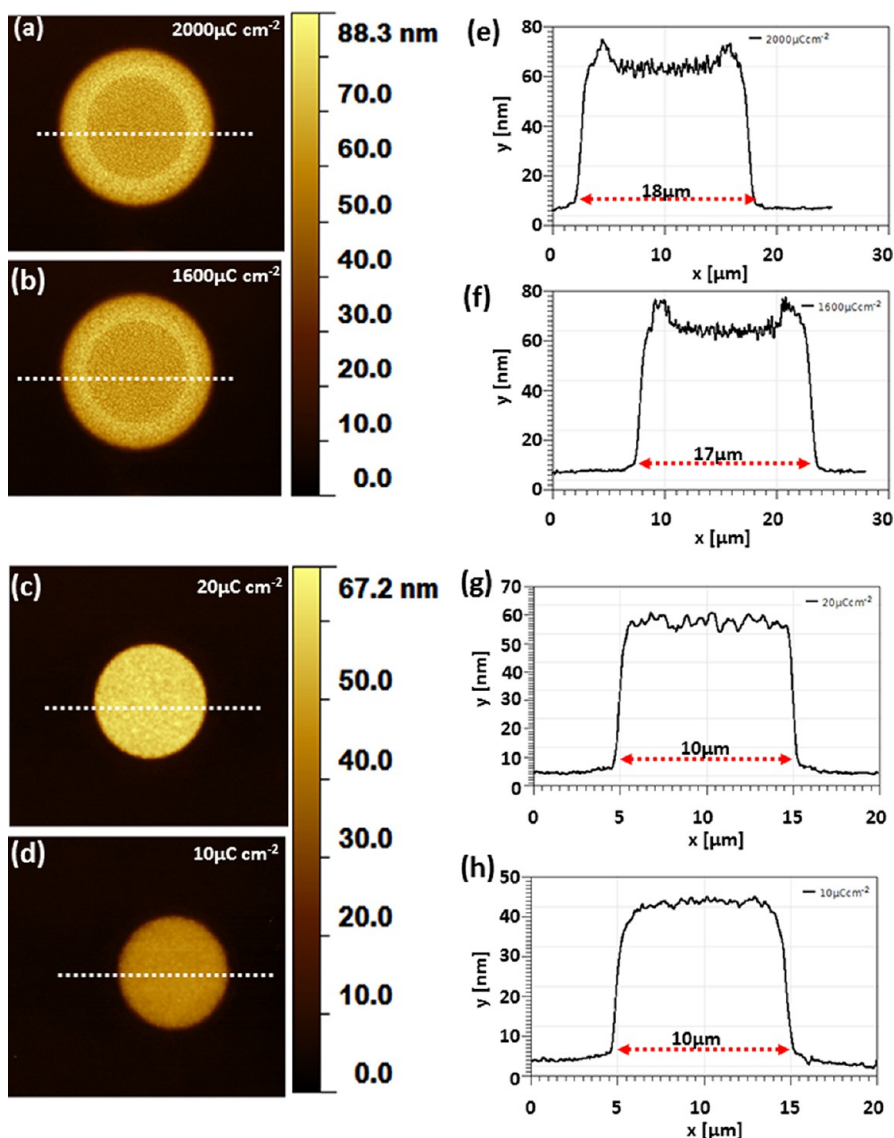
Figure 3. AFM images of QD-PEG micropatterns obtained *via* EBL. Circular disc shaped micropatterns created by EBL at (a) 2000 μC cm^{-2}, (b) 1600 μC cm^{-2}, (c) 20 μC cm^{-2} and (d) 10 μC cm^{-2} and their corresponding height profiles in panels e, f, g, and h, respectively.

micropatterns upon EBL, a series of electron beam dosages at gradual increments from 10 to 2000 μC cm^{-2} were tested at a constant electron acceleration voltage at 5 kV. For this purpose, QD-PEG micropattern arrays were fabricated in three different input shapes: disc shaped circle (radius of 5 μm), equilateral triangle (side length of 10 μm) and square box (width of 10 and 2 μm wall thickness). Scanning Electron Microscopy (SEM) images of the micropatterns revealed significant differences in fidelity in the obtained shapes compared to the original input dimensions of the micropatterns (Figure 2a). At dosages between 2000 and 50 μC cm^{-2}, low fidelity micropatterns were obtained, while at 20 and 10 μC cm^{-2}, the fidelity was the highest at all input micropatterns. The low fidelity observed at higher electron beam dosages is due to the electron beam proximity effect caused by electron beam scattering.[53]

Further, CLSM microscopy was used to assess the effect of electron beam dosage on the micropattern fidelity as well as on the fluorescence intensities of QD-PEG micropatterns. The effect of electron beam dosage on the micropattern fidelity with corresponding look-up table (LUT) for QD-PEG fluorescence intensities is presented in Figure 2b. At electron beam dosage of 50 μC cm^{-2} and above, we observed low fidelity in output micropatterns, while at electron beam dosages of 20 μC cm^{-2} and below, the fidelity was the highest. The CLSM results confirm the observations made using SEM of the patterns.

Further analysis of the fluorescence intensity LUT from Figure 2b shows higher florescence intensity for micropatterns created at 400 μC cm^{-2} and above. This phenomenon occurs possibly due to a larger number of QD-PEG cross-linked at higher electron beam
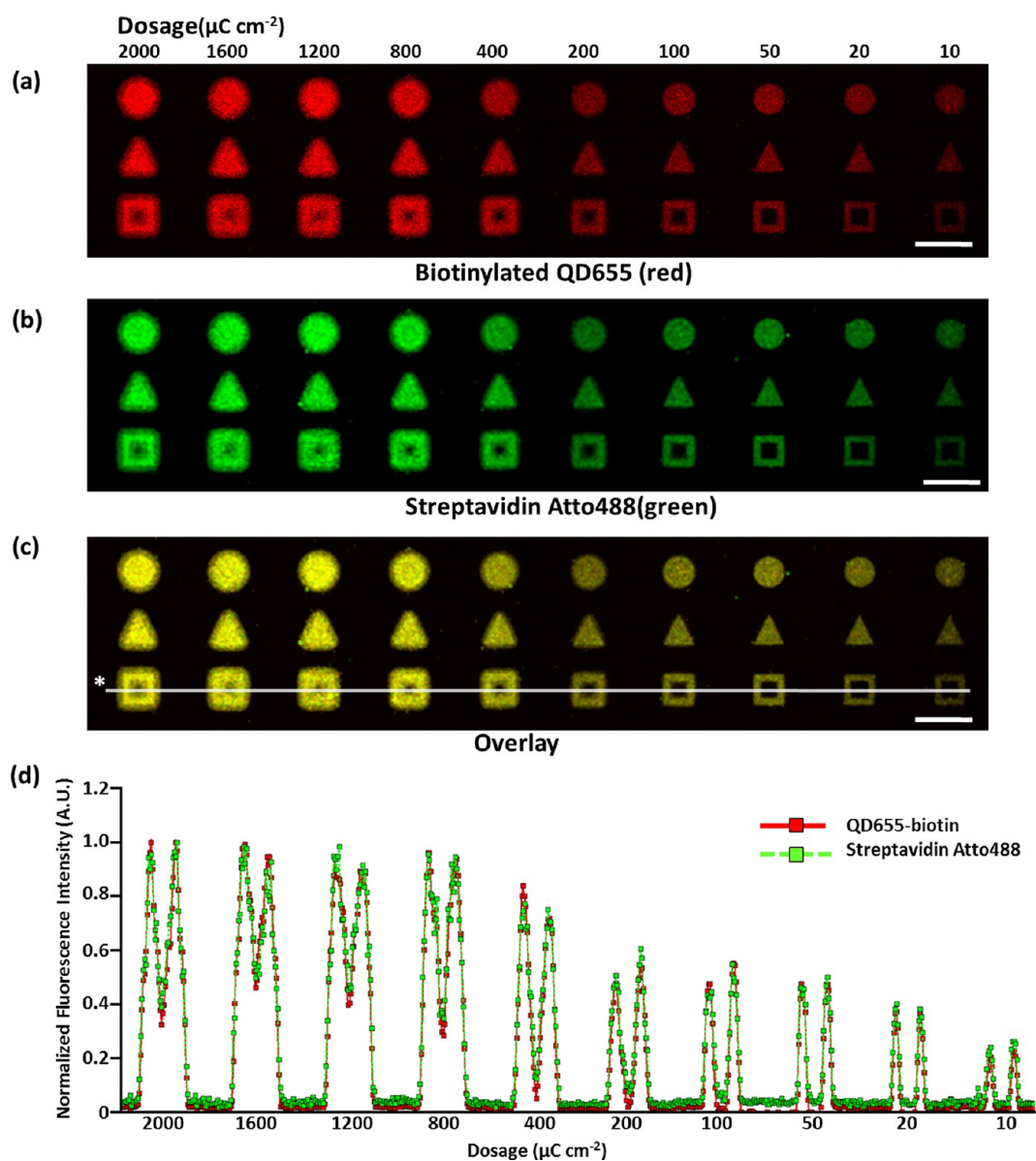
Figure 4. Functional characterization of QD-biotin micropatterns. CLSM fluorescence images of biotinylated QD patterns (a, red) to which streptavidin Atto488 (b, green) binds specifically and their overlay in panel c. Scale bar corresponds to 20 μm; (d) fluorescence intensity profile across overlay (* white line) in panel c.

dosages during EBL and not due to the enhancement of fluorescence caused by the close proximity of QDs to the gold layer on the substrate. Kulakovich *et al.* [54] They have shown that an optimal separation distance of 11 nm between QDs and gold is necessary to obtain fluorescence enhancement. At distances less than 6 nm and greater than 25 nm, no enhancement was observed. However, this enhancement depends primarily on the excitation wavelength that corresponds to the maximum of the plasmon resonance absorbance spectra of the colloid gold film ($\lambda = 550$ nm). In our approach, we used SAM of thiolated PEG ($M_w = 1000$) with a calculated length of ~4.5 nm and excitation wavelength of $\lambda = 405$ nm to excite QDs. Under these conditions, we did not observe fluorescence enhancement of QDs in the micropatterns. Nonetheless, the fluorescence

enhancement of QDs in such a hybrid pattern system could be achieved: (i) by varying the length of PEG-thiol that is used as a spacer between the gold layer on top of the substrate and the QD micropatterns and (ii) by using appropriate excitation wavelengths at plasmon resonance absorbance of gold. Such hybrid arrays can be used as efficient solid state light sources, nanobio interfaces and in bioanalytical devices.[55] We further quantified this effect from the CLSM images for the circular disc pattern (upper row in Figure 2b), and the results are shown in Figure 2c. It was found that above 20 μC cm^{-2} the area of cross-linking obtained by EBL exceeds the input dimension of the circular disc shaped micropattern of 5 μm in radius.

Further, atomic force microscopy (AFM) clarifies whether the electron beam dosage leads to differences

in the height profiles of the micropatterns, surface topology and fidelity. Figure 3 shows the AFM images of the circular disc shaped QD-PEG micropatterns obtained at higher and lower dosage of electron beam and their corresponding height profiles.

For high electron beam dosages of 2000 μC cm^{-2} (Figure 3a,e) and 1600 μC cm^{-2} (Figure 3b,f), a circular rim that is ~20 nm higher than the central circular area is observed. This rim is formed due to the electron scattering effect. The decrease in height of central area in comparison with the height of the rim occurs due to high cross-linking of PEG and possible destructive effect of high electron beam dosage on PEG. At lower dosages of 20 μC cm^{-2} (Figure 3c,g) and 10 μC cm^{-2} (Figure 3d,h), such an electron scattering effect and rim were not observed. However, we observed lower height (~45 nm) of the pattern at 10 μC cm^{-2} electron dosage in comparison with 20 μC cm^{-2} electron dosage (~60 nm) possibly due to the difference in cross-linking (weaker cross-linking at low electron dosage). The surface profile analyses of the AFM data for the circular disc shaped micropatterns along the dashed white lines in Figure 3a,b reveal that at high dosages of 2000 μC cm^{-2} (18 μm, Figure 3a,e) and 1600 μC cm^{-2} (17 μm, Figure 3b,f) the QD micropattern fidelity is lower than at low electron beam dosages of 20 μC cm^{-2} (10 μm, Figure 3c,g) and 10 μC cm^{-2} (10 μm, Figure 3d,h). These observations highlight the drawback of using high electron beam dosages[56] resulting in strong electron scattering leading to off target cross-linking and low fidelity patterns. Thus, by using low electron beam dosage during EBL patterning, high fidelity patterns can be created. AFM results together with SEM and CLSM studies confirm our observations that at 20 μC cm^{-2} high fidelity QD micropattern arrays are obtained.

Biotinylated QDs Retain Their Activity and Bind Specifically to Streptavidin upon EBL. For creating functional micropatterns using EBL, it is essential to investigate the effect of the electron beam on the activity of the molecule to be immobilized into the patterns. Because detection systems based on biotin and streptavidin interactions are common, robust and widely used in analyte capture and sensing, we chose to use biotinylated QDs (QD-biotin) for micropatterning using EBL. We used electron beam dosages from 10 up to 2000 μC cm^{-2} to assess the suitability of QD-biotin for creating micropatterns and to investigate the effect of electron dosage on QD-biotin conjugates to capture and detect streptavidin.

CLSM images of the QD-biotin micropatterns and the detection of the biotin on the QDs through fluorescently labeled streptavidin can be seen in Figure 4a and Figure 4b, respectively.

An overlay of fluorescence signals from QD-biotin (Figure 4a, red) and streptavidin Atto488 (Figure 4b, green) reveals the specific binding of streptavidin
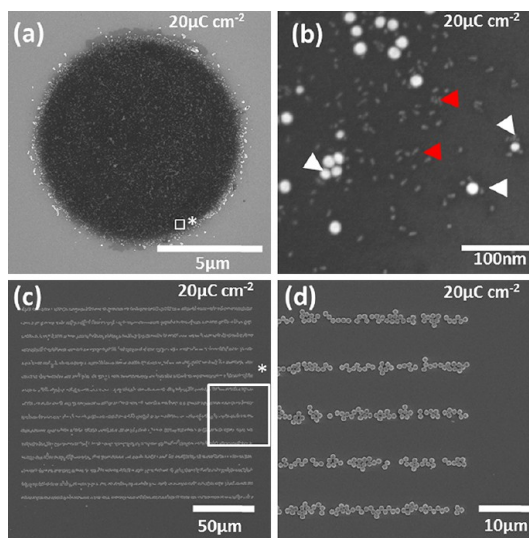

Figure 5. (a) SEM image of biotinylated 20 nm gold nanoparticles bound to QD-biotin micropattern; (b) high resolution magnification of the white box in panel a. Biotinylated gold nanoparticles (white arrow) bind to QD-biotin (red arrow) micropattern through streptavidin as a linker protein. (c) SEM image of specific capture of streptavidin-coated 1 μm magnetic beads bound to QD-biotin line patterns of 2 μm width and a pitch of 10 μm; (d) high resolution magnification of the white box in panel c.

Atto488 to the QD-biotin micropatterns. In addition, Figure 4d shows the fluorescence profile across the open box patterns from Figure 4c which reveals a high fluorescence signal for QD patterns at dosages of 2000, 1600, 1200, and 800 μC cm^{-2}, while from 400 down to 10 μC cm^{-2}, the fluorescence intensity decreases. This phenomenon is possibly related to the retention of a higher number of QD-biotin within the cross-linked PEG matrix at higher electron dosages upon rinsing. SEM provides further evidence that streptavidin is bound to the QD-biotin in a sandwich assay where biotinylated 20 nm gold nanoparticles were co-incubated with QD-biotin micropatterns following the incubation with streptavidin (Figure 4b). Figure 5a shows the circular disc shaped pattern of QD-biotin bound to 20 nm biotinylated gold nanoparticles through streptavidin as an intermediate linker.

At higher magnification of the same pattern it is possible to clearly see a close association of biotinylated 20 nm gold nanoparticles (white arrowhead) to QD-biotin (red arrowhead) due to the presence of streptavidin as a linker molecule (Figure 5b). Furthermore, we used 1 μm in diameter magnetic beads functionalized with streptavidin to demonstrate the feasibility of a bead capture system on line patterns of QD-biotin (Figure 5c,d). To achieve this, parallel line patterns of QD-biotin with a line width of 2 μm and a pitch distance of 10 μm were created at electron beam dosages of 20, 50, 100, 200, and 1000 μC cm^{-2} (Figure S1). From Figure 5c,d, it is clear that at 20 μC cm^{-2} electron beam dosage, streptavidin functionalized
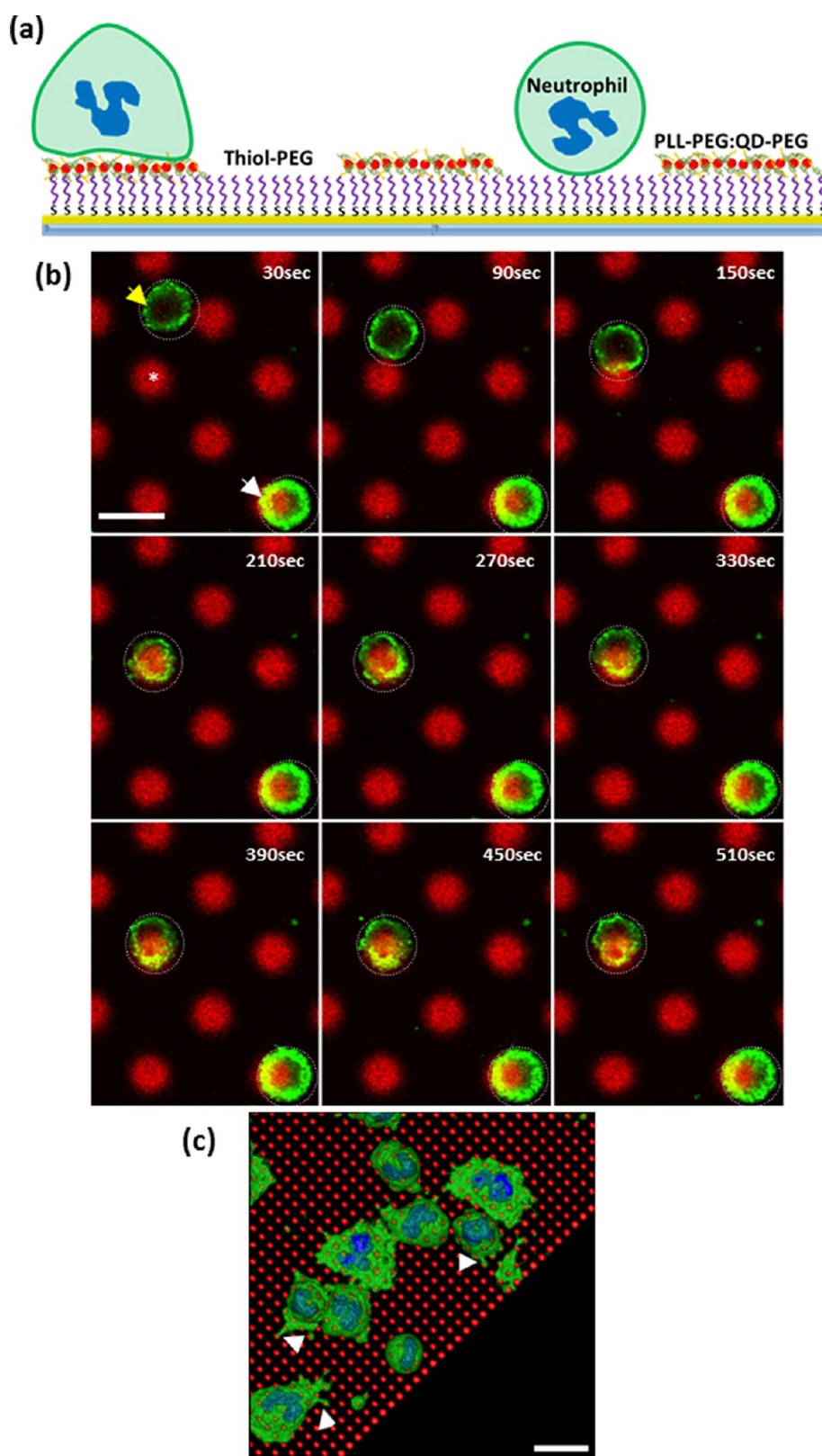
Figure 6. Neutrophils adhere to the PLL-PEG:QD-PEG micropattern. (a) Schematics of adherence of neutrophils on PLL-PEG: QD-PEG micropatterns; (b) live cell time-lapse CLSM images of specific attachment of neutrophils (green) on PLL-PEG:QD-PEG circular disc shaped patterns of 5 μm in diameter (red). Scale bar corresponds to 10 μm. (c) 3D iso-surface image of confocal Z stack of neutrophils (green membrane dye and blue nucleus) on disc shaped micropatterns of 2 μm in diameter of PLL-PEG: QD-PEG (red). Scale bars correspond to 10 μm.
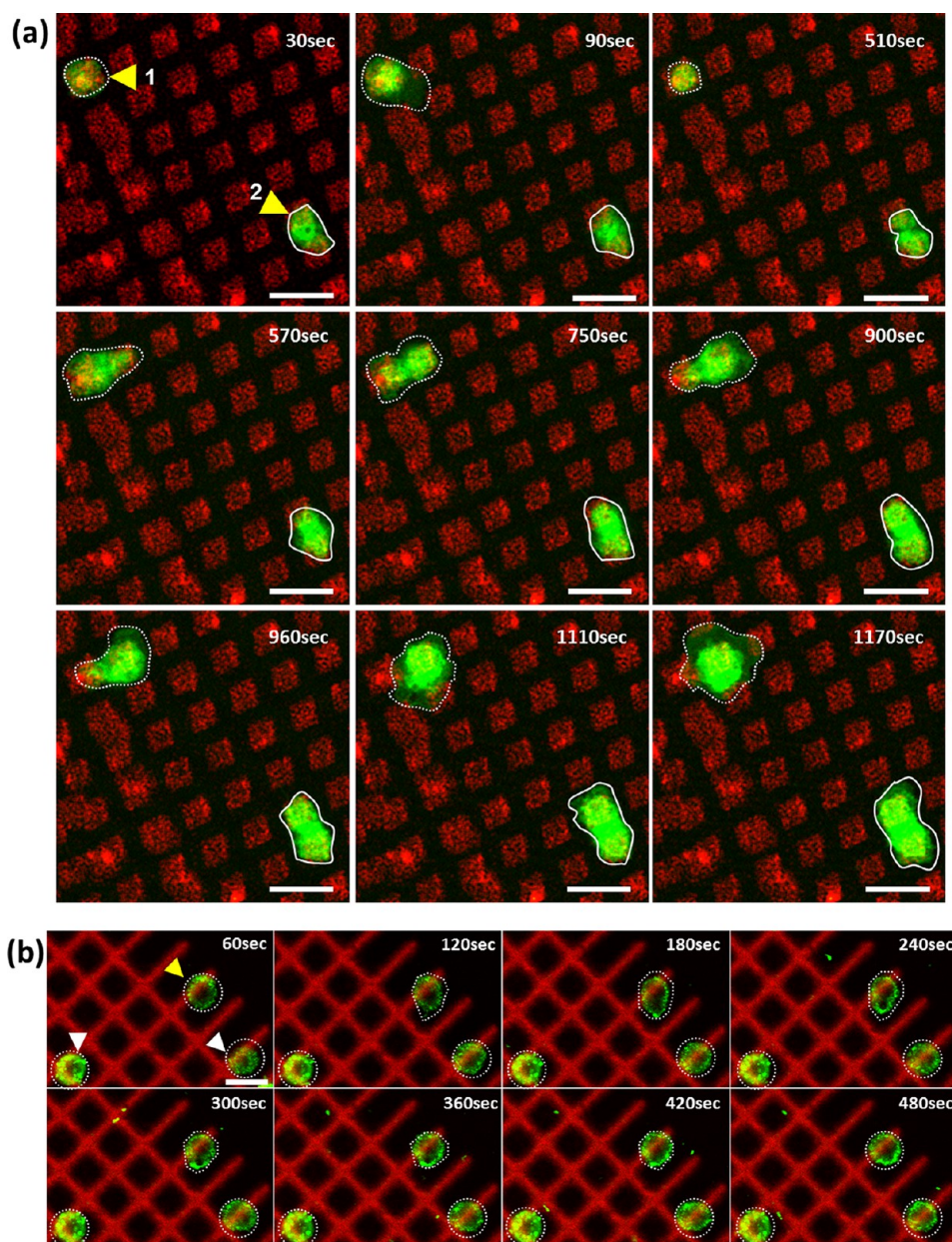
Figure 7. Neutrophils spreading and migration on PLL-PEG:QD-PEG micropatterns. Live cell CLSM images of neutrophils (green, indicated by yellow arrowhead) adhering, spreading and migrating on PLL-PEG:QD-PEG (red) square shaped patterns (a) and on grid-like PLL-PEG:QD-PEG micropattern arrays (indicated by white arrowhead) (b). Scale bar is (a) 12.5 μm and (b) 10 μm.

magnetic microbeads bind specifically to the line patterns of QD-biotin. This was also observed at higher electron beam dosages and is due to the enhanced electron beam backscattering (Figure S2). The possibility to capture, immobilize and form well-defined arrays of large objects such as beads, organelles, and cells opens up new avenues for the use of EBL micropatterns of QDs for designing novel optical reporter systems.

Adhesion and Spreading of Neutrophils on Hybrid PLL-PEG: QD-PEG Micropatterned Surfaces. As a proof-of-concept that our hybrid quantum dot microarrays can be used for cell adhesion and cell migration studies,

we investigated the behavior of neutrophils, one of the most abundant and most important cells in blood, upon their contact with PLL-PEG:QD-PEG micropatterned surfaces (see Figure 6a) of different geometries and pitch sizes. PLL (positively charged) is routinely used to enhance cell attachment. To confer cell adhesive properties to the QD microarrays, PLL-PEG was incorporated into the micropatterns. The initial interaction between neutrophils and PLL-PEG-QD-PEG patterns leading to neutrophil adherence is electrostatically driven (positively charged PLL and negatively charged cell membrane). At later stages (neutrophil spreading and migration), there might be

an influence of the cross-linking density, surface roughness and stiffness of the substrate[57] on the cellular dynamics. The effectiveness of the PLL-PEG: QD-PEG micropatterns to adhere and immobilize neutrophils was tested using live cell CLSM. We further tested the feasibility of the PLL-PEG:QD-PEG micropatterns to capture and immobilize neutrophils on circular disc-like micropatterns. In Figure 6b, the CLSM live cell image sequence of neutrophil adherence specifically on circular disc shaped micropatterns of 2.5 μm radius shows two cells of which one (white arrowhead) is already adhered and immobilized on the PLL-PEG:QD-PEG micropattern, while another one (yellow arrowhead) is not adherent to the micropattern at 30 and 90 s image intervals (see Movie 1 in Supporting Information). At 150 s, the nonadherent neutrophil comes in contact with the micropattern and then establishes a complete contact at 210 s and remains adherent at 510 s. Figure 6c shows a 3D isosurface rendered image of confocal fluorescence microscopy Z stacks of neutrophils adhering on circular disc-like PLL-PEG:QD-PEG micropatterns of 1.25 μm in diameter separated by a pitch of 1 μm. We observed no difference between the two circular disc-like PLL-PEG:QD-PEG micropatterns in their ability to capture and immobilize neutrophils.

Next, we aimed to study the influence of the PLL-PEG:QD-PEG micropattern geometry (square, circle, grid-like) and their spatial arrangement (pitch distance) on the adhesion, spreading and migration of neutrophils. In Figure 7a, selected live cell time-lapse CLSM images of two neutrophils (numbered 1 and 2, yellow arrowheads) on square patterns of side length 5 μm and a pitch distance of 2.5 μm shows the dynamics of adherence, gradual shape changes during spreading and migration of neutrophils on PLL-PEG:QD-PEG micropatterns (for complete image sequence see Movie 2 in Supporting Information). We observed that at 30 s the neutrophils have established contact with the micropattern. However, at 90 s one of the neutrophils (numbered 1, Figure 7a) spreads out the plasma membrane that reaches beyond the PLL-PEG:QD-PEG micropattern onto the SAM layer of PEG-thiol and then, at 510 s the plasma membrane is completely retracted to the original position on the micropattern. From 570 until 1170 s, dramatic changes in the neutrophil morphology were observed. The neutrophil extends its plasma membrane over the neighboring PLL-PEG:QD-PEG micropattern and then migrates completely to the next pattern. In addition, during this migration process from 960 to 1170 s, the neutrophil numbered 1 is constantly extending its plasma membrane to the neighboring micropatterns. Furthermore, another neutrophil (numbered 2, Figure 7a) shows adherence and spreading behavior, wherein it spreads between two adjacent micropatterns with time. During the

spreading and migration of neutrophils on square micropatterns, different cell morphologies were observed: spherical neutrophils were found on the PLL-PEG:QD-PEG lacking surface, while spreading neutrophils were seen specifically on the PLL-PEG:QD-PEG micropattern (Figure S3).

To further investigate whether such a spreading and migration behavior exhibited by neutrophils on PLL-PEG:QD-PEG micropatterns is restricted to the dimensions and the pitch between the patterns, using EBL we created grid-like patterns with a line width of 2 μm and a pitch distance of 10 μm. In Figure 7b, live cell time lapse CLSM images of the neutrophils on such patterns are shown (see Movie 3 in Supporting Information). We observe that at 60 s the neutrophils (indicated by white and yellow arrowhead) adhere specifically on the lines of the grid-like pattern. Between 120 and 180 s, one of the neutrophils (yellow arrowhead) starts to exhibit migratory behavior which ceases from 240 s onward and the neutrophil comes back to the initial position on the grid. These results demonstrate that the PLL-PEG:QD-PEG micropattern dimensions and their pitch distances influence the spreading and migratory behavior of neutrophils. Such micropattern arrays created with EBL can be used to investigate cellular behavior related to adhesion, spreading and migration in a wide range of cell types.

CONCLUSIONS

In summary, we have reported on a new microfabrication strategy to generate high fidelity prefunctionalized water-soluble QD micropattern arrays using EBL. We have shown that tuning of the electron beam dosage is an important factor to create high fidelity QD micropatterns. Low electron beam dosage of 20 μC cm^{-2} at electron acceleration voltage of 5 kV is optimal to achieve high fidelity micropatterns for all investigated QDs and their conjugates. Furthermore, the possibility to detect and capture gold nanoparticles and magnetic microbeads using the specific streptavidin—biotin interaction on QD micropatterns opens new avenues for generating bottom-up hybrid nano- and microstructures. We also demonstrated that human blood derived neutrophils can be captured on QD micropatterns of varying geometries. Neutrophils adhere on all geometric shapes of PLL-PEG:QD-PEG micropatterns and exhibit preferential migratory behavior to the neighboring patterns. On grid-like patterns with 1 μm width and a pitch distance of 10 μm, they adhere but do not migrate to the neighboring patterns compared to those neutrophils on square patterns of 5 μm side length with a pitch of 2.5 μm. These observations will assist in designing nano-biointerface tools to create functional fluorescent patterns required for FRET based studies to probe cellular adhesion, migration and to investigate the role of spatial distance, nanotopological cues and their

influence on the control of cellular signaling pathways. In the future, these QD micropatterned surfaces can be integrated into microfluidic platforms that can be used to detect analytes and to investigate the influence of shear stress on cell dynamics using quantitative fluorescence readouts.

METHODS

Chemicals and Reagents. PLL(20)-g[3.5]-PEG(2) was purchased from SuSos AG, Dübendorf, Switzerland. Water-soluble QDot 655 ITK Amino (PEG) Quantum Dots and QDot 655 Biotin Conjugate were from Molecular Probes. Streptavidin Atto 488 was purchased from Attotec GmbH, Siegen, Germany. 2-[Methoxy(polyethyleneoxy)propyl]trimethoxysilane (6–9 PE-units, CAS no. 65994-07-2) PEG-silane was from ABCR GmbH & Co. Karlsruhe, Germany. Triethilamine and (poly(ethylene glycol) methyl ether thiol, catalog no. 729108) PEG-thiol were purchased from Sigma-Aldrich, Germany. Biotin-PEG-SH was supplied by Iris Biotech GmbH, Germany. The 1 μm magnetic streptavidin coated beads Dynabeads MyOne Streptavidin C1 were from Invitrogen. 4',6-Diamidino-2-phenylindole dihydrochloride (DAPI, catalog no. D9542) was from Sigma-Aldrich, Germany. The 20 nm gold nanoparticles were a kind gift from Dr. Ali Abou-Hassan from the PECSA Lab at the University Pierre et Marie Curie, Paris, France.

Fabrication of QD Microarrays and Patterns. The 24 mm round glass coverslips (Plano GmbH, Germany) were cleaned using Standard Clean 1 (SC-1 step) of RCA cleaning (a 1:1:5 solution of NH$_4$OH (ammonium hydroxide):H$_2$O$_2$ (hydrogen peroxide):H$_2$O (water) at 70 °C for 10 min). The RCA cleaned glass coverslips were dried under nitrogen stream, cleaned for 10 min with oxygen plasma (600W, oxygen flow 500 sccm, Gigabatch 310, PVA TePla, Germany) and then sputter coated (Q150R S, Quorum Technologies, United Kingdom) with gold to create a conductive layer. The 10 × 10 mm silicone chips (Plano GmbH, Germany) were cleaned similarly, except for the gold coating step. To create a nonadhesive layer, gold coated glass coverslips were functionalized with PEG-thiol (5 mg/mL of PEG-thiol in absolute ethanol) for 2 h, washed with ethanol and dried with a nitrogen stream. Silicon chips were functionalized with PEG-silane (1% (v/v) PEG-silane + 1% (v/v) triethylamine in absolute toluene) for 2 h, washed in absolute toluene and dried under a nitrogen stream. To create patterned microarrays, a suspension of 100 nM PEG-QD655 and 1% (w/v) PEG-PLL in 80% 2-propanol was spin-coated (DELTA6 RC TT, Süss Micro Tec, Germany) for 60 s at 2000 rpm on glass coverslip and silicone chips. Electron Beam Lithography was performed in a Zeiss Supra 40 VP scanning electron Microscope equipped with an ELPHY Quantum EBL system (Raith GmbH, Germany). As a preliminary step for EBL processing, for an efficient cross-linking of QDs, the electron beam dosage was optimized. A range of dosage exposures (10–2000 μC cm^{-2}) were tested to obtain the optimum dosage required to generate stable QD based micropattern array features without excessive degradation and overexposure of QDs.

Atomic Force Microscopy (AFM) Characterization of QD Patterns. An AFM NanoWizard 3 AFM System (JPK Instruments AG, Berlin, Germany) coupled to an inverted Olympus ix81 microscope (Hamburg, Germany) was used. AFM silicon tips (type TESP with a spring constant of 42 N/m, Veeco, Santa Barbara, CA) were used for the imaging experiments. The glass coverslip with QD patterned arrays was fixed in a BioCellTM (JPK Instruments AG, Berlin, Germany) and the area of interest was identified using the inverted microscope. The imaging was performed in air using the software JPK SPM Control Software V.4. The following conditions were used for imaging: tapping mode (AC mode); line rate, 0.1 Hz; and pixel, 1024 × 1024. Different area sizes were imaged: 60 μm × 60 μm, 85 μm × 85 μm, and 100 μm × 100 μm. AFM data visualization and analysis was performed with Gwyddion version 2.3 software.

Elipsometry. The thickness of spin-coated PLL-PEG:QDs layer was measured with the spectroscopic imaging elipsometer Nanofilm_ep3se (Accurion GmbH, Germany). All measurements were carried out at a single angle of incident of 42° vertical to the surface and in a spectral range of 360–900 nm. Afterward, the amplitude (ψ) and phase (Δ) data sets were fitted with Accurion EP4_model software (Accurion GmbH, Germany). The measurements were repeated at least three times in different regions of the sample.

Colloidal Gold Labeling. The 20 nm colloidal gold nanoparticles were incubated with biotin-PEG-SH for 1 h at room temperature. Unconjugated biotin was washed away from biotinylated colloidal gold by centrifugation at 10 000 rpm for 10 min. The biotin–gold nanoparticle conjugate was stored at 4 °C until further use.

Neutrophil Isolation and Live Cell Imaging. Heparinized whole blood (20–30 mL) was collected from healthy human donors. After dextran sedimentation, granulocytes were isolated from the supernatant leukocyte-rich plasma by Ficoll-Hypaque gradient centrifugation and red blood cells were lysed with ammonium chloride solution. Neutrophils were labeled with Oregon Green 488 1,2-dihexadecanoyl-sn-glycero-3-phosphoethanolamine (Molecular Probes, Invitrogen). Neutrophils were imaged live in the presence of RPMI 1640 (cat. no. 27016-021, Gibco-Invitrogen) supplemented with 5% (v/v) low endotoxin human serum albumin (cat. no. 800-126P, Gemini Bioproducts) at a seeding density of 10^3 cells/mL. Live cell confocal laser scanning microscopy was carried out at 37 °C under controlled atmosphere on an Olympus FLUOVIEW FV1000. Image processing was performed with ImageJ (Rasband, W. S., ImageJ, U.S. National Institutes of Health, Bethesda, MD, 1997–2012, http://imagej.nih.gov/ij/.) and Imaris (Bitplane AG, Zurich, Switzerland).

Conflict of Interest: The authors declare no competing financial interest.

Supporting Information Available: The influence of electron beam dosage and electron backscattering on the fidelity of QD-biotin line patterns. The influence of electron beam dosage and electron backscattering on the capture of streptavidin coated magnetic microbeads to QD-biotin line patterns. SEM image of neutrophils spreading on QD micropatterns. Three movies showing the migration of neutrophils on QD patterns of different shapes. This material is available free of charge *via* the Internet at http://pubs.acs.org.

REFERENCES AND NOTES

1. Stevens, M. M.; George, J. H. Exploring and Engineering the Cell Surface Interface. *Science* **2005**, *310*, 1135–1138.
2. Langer, R.; Tirrell, D. A. Designing Materials for Biology and Medicine. *Nature* **2004**, *428*, 487–492.
3. Discher, D. E.; Mooney, D. J.; Zandstra, P. W. Growth Factors, Matrices, and Forces Combine and Control Stem Cells. *Science* **2009**, *324*, 1673–1677.
4. Crescitelli, A.; Ricciardi, A.; Consales, M.; Esposito, E.; Granata, C.; Galdi, V.; Cutolo, A.; Cusano, A. Nanostructured Metallo-Dielectric Quasi-Crystals: Towards Photonic-Plasmonic Resonance Engineering. *Adv. Funct. Mater.* **2012**, *22*, 4389–4398.

5. Fiddes, L. K.; Chan, H. K. C.; Lau, B.; Kumacheva, E.; Wheeler, A. R. Durable, Region-Specific Protein Patterning in Microfluidic Channels. *Biomaterials* **2010**, *31*, 315–320.

6. Ziauddin, J.; Sabatini, D. M. Microarrays of Cells Expressing Defined cDNAs. *Nature* **2001**, *411*, 107–110.

7. Hahn, M. S.; Miller, J. S.; West, J. L. Three-Dimensional Biochemical and Biomechanical Patterning of Hydrogels for Guiding Cell Behavior. *Adv. Mater.* **2006**, *18*, 2679–2684.

8. Flemming, R. G.; Murphy, C. J.; Abrams, G. A.; Goodman, S. L.; Nealey, P. F. Effects of Synthetic Micro- and Nano-Structured Surfaces on Cell Behavior. *Biomaterials* **1999**, *20*, 573–588.

9. Alivisatos, A. P. Semiconductor Clusters, Nanocrystals and Quantum Dots. *Science* **1996**, *271*, 933–937.

10. Chan, Y. T.; Snee, P. T.; Caruge, J. M.; Yen, B. K.; Nair, G. P.; Nocera, D. G.; Bawendi, M. G. A Solvent-Stable Nano-crystal-Silica Composite Laser. *J. Am. Chem. Soc.* **2006**, *128*, 3146–3147.

11. Huynh, W. U.; Dittmer, J. J.; Alivisatos, A. P. Hybrid Nanorod-Polymer Solar Cells. *Science* **2002**, *295*, 2425–2427.

12. Taylor, Z. R.; Sanchez, E. S.; Keay, J. C.; Johnson, M. B.; Schmidtke, D. W. Patterning of Quantum Dot Bioconjugates *via* Particle Lithography. *Langmuir* **2010**, *26*, 18938–18944.

13. Lewandowski, B. R.; Kelley, A. T.; Singleton, R.; Li, J. R.; Lowry, M.; Warner, I. M.; Garno, J. C. Nanostructures of Cysteine-Coated CdS Nanoparticles Produced with "Two-Particle" Lithography. *J. Phys. Chem. C* **2009**, *113*, 5933–5940.

14. Gokarna, A.; Jin, L. H.; Hwang, J. S.; Cho, Y. H.; Lim, Y. T.; Chung, B. H.; Youn, S. H.; Choi, D. S.; Lim, J. H. Quantum Dot-based Protein Micro- and Nanoarrays for Detection of Prostate Cancer Biomarkers. *Proteomics* **2008**, *8*, 1809–1818.

15. Rakickas, T.; Gavutis, M.; Reichel, A.; Piehler, J.; Liedberg, B.; Valiokas, R. Protein−Protein Interactions in Reversibly Assembled Nanopatterns. *Nano Lett.* **2008**, *8*, 3369–3375.

16. Gassensmith, J. J.; Erne, P. M.; Paxton, W. F.; Frasconi, M.; Donakowski, M. D.; Stoddart, J. F. Patterned Assembly of Quantum Dots onto Surfaces Modified with Click Micro-contact Printing. *Adv. Mater.* **2013**, *25*, 223–226.

17. Hoa, X. D.; Martin, M.; Jimenez, A.; Beauvais, J.; Charette, P.; Kirk, A.; Tabrizian, M. Fabrication and Characterization of Patterned Immobilization of Quantum Dots on Metallic Nano-Gratings. *Biosens. Bioelectron.* **2008**, *24*, 970–975.

18. Kramer, R. K.; Pholchai, N.; Sorger, V. J.; Yim, T. J.; Oulton, R.; Zhang, X. Positioning of Quantum Dots on Metallic Nanostructures. *Nanotechnology* **2010**, *21*, 145307.

19. Nandwana, V.; Subramani, C.; Yeh, Y. C.; Yang, B. Q.; Dickert, S.; Barnes, M. D.; Tuominen, M. T.; Rotello, V. M. Direct Patterning of Quantum Dot Nanostructures *via* Electron Beam Lithography. *J. Mater. Chem.* **2011**, *21*, 16859–16862.

20. Nandwana, V.; Mout, R.; Yeh, Y.-C.; Dickert, S.; Tuominen, M.; Rotello, V. Patterning of Protein/Quantum Dot Hybrid Bionanostructures. *J. Inorg. Organomet. Polym.* **2013**, *23*, 227–232.

21. Verma, V. B.; Stevens, M. J.; Silverman, K. L.; Dias, N. L.; Garg, A.; Coleman, J. J.; Mirin, R. P. Time-Resolved Photoluminescence of Lithographically Defined Quantum Dots Fabricated by Electron Beam Lithography and Wet Chemical Etching. *J. Appl. Phys.* **2011**, *109*, 123112–123110.

22. Yu, W. W.; Chang, E.; Drezek, R.; Colvin, V. L. Water-Soluble Quantum Dots for Biomedical Applications. *Biochem. Biophys. Res. Commun.* **2006**, *348*, 781–786.

23. Andrade, J. J.; Brasil, A. G.; Barbosa, B. J. A. P.; Azevedo, C. A.; Leite, E. S.; Farias, P. M. A.; Fontes, A.; Santos, B. S. Biocompatible Water Soluble UV-Blue Emitting ZnSe Quantum Dots for Biomedical Applications. *Proc. SPIE* **2010**, *7575* , No. 757507 .

24. Janczewski, D.; Tomczak, N.; Han, M. Y.; Vancso, G. J. Synthesis of Functionalized Amphiphilic Polymers for Coating Quantum Dots. *Nat. Protoc.* **2011**, *6*, 1546–1553.

25. Susumu, K.; Mei, B. C.; Mattoussi, H. Multifunctional Ligands Based on Dihydrolipoic Acid and Polyethylene Glycol to Promote Biocompatibility of Quantum Dots. *Nat. Protoc.* **2009**, *4*, 424–436.

26. Mei, B. C.; Susumu, K.; Medintz, I. L.; Mattoussi, H. Poly-ethylene Glycol-based Bidentate Ligands to Enhance Quantum Dot and Gold Nanoparticle Stability in Biological Media. *Nat. Protoc.* **2009**, *4*, 412–423.

27. Janczewski, D.; Tomczak, N.; Song, J.; Long, H.; Han, M. Y.; Vancso, G. J. Fabrication and Responsive Behaviour of Quantum Dot/PNIPAM Micropatterns Obtained by Template Copolymerization in Water. *J. Mater. Chem.* **2011**, *21*, 6487–6490.

28. Khalid, W.; El Helou, M.; Murbock, T.; Yue, Z.; Montenegro, J. M.; Schubert, K.; Gobel, G.; Lisdat, F.; Witte, G.; Parak, W. J. Immobilization of Quantum Dots *via* Conjugated Self-Assembled Monolayers and Their Application as a Light-Controlled Sensor for the Detection of Hydrogen Peroxide. *ACS Nano* **2011**, *5*, 9870–9876.

29. Kolesnikova, T. A.; Kohler, D.; Skirtach, A. G.; Möhwald, H. Laser-Induced Cell Detachment, Patterning, and Re-growth on Gold Nanoparticle Functionalized Surfaces. *ACS Nano* **2012**, *6*, 9585–9595.

30. Krauss, T. N.; Barrena, E.; Lohmuller, T.; Spatz, J. P.; Dosch, H. Growth Mechanisms of Phthalocyanine Nanowires Induced by Au Nanoparticle Templates. *Phys. Chem. Ch. Ph.* **2011**, *13*, 5940–5944.

31. Maus, L.; Dick, O.; Bading, H.; Spatz, J. P.; Fiammengo, R. Conjugation of Peptides to the Passivation Shell of Gold Nanoparticles for Targeting of Cell-Surface Receptors. *ACS Nano* **2010**, *4*, 6617–6628.

32. Nguyen, M. N.; Lebarbe, T.; Zouani, O. F.; Pichavant, L.; Durrieu, M. C.; Heroguez, V. Impact of RGD Nanopatterns Grafted onto Titanium on Osteoblastic Cell Adhesion. *Biomacromolecules* **2012**, *13*, 896–904.

33. Hanske, C.; Muller, M. B.; Bieber, V.; Tebbe, M.; Jessl, S.; Wittemann, A.; Fery, A. The Role of Substrate Wettability in Nanoparticle Transfer from Wrinkled Elastomers: Fundamentals and Application toward Hierarchical Patterning. *Langmuir* **2012**, *28*, 16745–16750.

34. Schweikart, A.; Pazos-Perez, N.; Alvarez-Puebla, R. A.; Fery, A. Controlling Inter-Nanoparticle Coupling by Wrinkle-Assisted Assembly. *Soft Matter* **2011**, *7*, 4093–4100.

35. Gu, W.; Pellegrino, T.; Parak, W. J.; Boudreau, R.; Le Gros, M. A.; Gerion, D.; Alivisatos, A. P.; Larabell, C. A. Quantum-Dot-Based Cell Motility Assay. *Sci. STKE* **2005**, l5.

36. Pellegrino, T.; Parak, W. J.; Boudreau, R.; Le Gros, M. A.; Gerion, D.; Alivisatos, A. P.; Larabell, C. A. Quantum Dot-based Cell Motility Assay. *Differentiation* **2003**, *71*, 542–548.

37. Amulic, B.; Cazalet, C.; Hayes, G. L.; Metzler, K. D.; Zychlinsky, A. Neutrophil Function: From Mechanisms to Disease. *Annu. Rev. Immunol.* **2012**, *30*, 459–489.

38. Segal, A. W. How Neutrophils Kill Microbes. *Annu. Rev. Immunol.* **2005**, *23*, 197–223.

39. Coghill, P. A.; Kesselhuth, E. K.; Shimp, E. A.; Khismatullin, D. B.; Schmidtke, D. W. Effects of Microfluidic Channel Geometry on Leukocyte Rolling Assays. *Biomed. Microdevices* **2013**, *15*, 183–193.

40. Nalayanda, D. D.; Kalukanimuttam, M.; Schmidtke, D. W. Micropatterned Surfaces for Controlling Cell Adhesion and Rolling under Flow. *Biomed. Microdevices* **2007**, *9*, 207–214.

41. Taylor, Z. R.; Keay, J. C.; Sanchez, E. S.; Johnson, M. B.; Schmidtke, D. W. Independently Controlling Protein Dot Size and Spacing in Particle Lithography. *Langmuir* **2012**, *28*, 9656–9663.

42. Tan, J.; Saltzman, W. M. Topographical Control of Human Neutrophil Motility on Micropatterned Materials with Various Surface Chemistry. *Biomaterials* **2002**, *23*, 3215–3225.

43. Tan, J.; Shen, H.; Saltzman, W. M. Micron-Scale Positioning of Features Influences the Rate of Polymorphonuclear Leukocyte Migration. *Biophys. J.* **2001**, *81*, 2569–2579.

44. Tan, J.; Shen, H.; Carter, K. L.; Saltzman, W. M. Controlling Human Polymorphonuclear Leukocytes Motility Using Microfabrication Technology. *J. Biomed. Mater. Res.* **2000**, *51*, 694–702.

45. del Campo, A.; Arzt, E. Fabrication Approaches for Generating Complex Micro- and Nanopatterns on Polymeric Surfaces. *Chem. Rev.* **2008**, *108*, 911–945.

46. Hwang, E.; Smolyaninov, I. I.; Davis, C. C. Surface Plasmon Polariton Enhanced Fluorescence from Quantum Dots on Nanostructured Metal Surfaces. *Nano Lett.* **2010**, *10*, 813–820.

47. Park, Y.; Roh, Y. G.; Kim, U. J.; Chung, D. Y.; Suh, H.; Kim, J.; Cheon, S.; Lee, J.; Kim, T. H.; Cho, K. S.; Lee, C. W. Nanoscale Patterning of Colloidal Quantum Dots on Transparent and Metallic Planar Surfaces. *Nanotechnology* **2012**, *23*, 355302.

48. Revzin, A.; Tompkins, R. G.; Toner, M. Surface Engineering with Poly(ethylene glycol) Photolithography To Create High-Density Cell Arrays on Glass. *Langmuir* **2003**, *19*, 9855–9862.

49. Bae, M.; Divan, R.; Suthar, K. J.; Mancini, D. C.; Gemeinhart, R. A. Fabrication of Poly(ethylene glycol) Hydrogel Structures for Pharmaceutical Applications using Electron beam and Optical Lithography. *J. Vac. Sci Technol., B* **2010**, *28*, C6P24–C6P29.

50. Golzhauser, A.; Geyer, W.; Stadler, V.; Eck, W.; Grunze, M.; Edinger, K.; Weimann, T.; Hinze, P. Nanoscale Patterning of Self-Assembled Monolayers with Electrons. *J. Vac. Sci. Technol., B* **2000**, *18*, 3414–3418.

51. Turchanin, A.; Tinazli, A.; El-Desawy, M.; Grossann, H.; Schnietz, M.; Solak, H. H.; Tampe, R.; Golzhauser, A. Molecular Self-Assembly, Chemical Lithography, and Biochemical Tweezers: A Path for the Fabrication of Functional Nanometer-Scale Protein Arrays. *Adv. Mater.* **2008**, *20*, 471–477.

52. Kuller, A.; El-Desawy, M. A.; Stadler, V.; Geyer, W.; Eck, W.; Golzhauser, A. Electron-Beam Lithography with Aromatic Self-Assembled Monolayers on Silicon Surfaces. *J. Vac. Sci. Technol., B* **2004**, *22*, 1114–1117.

53. Rundqvist, J.; Hoh, J. H.; Haviland, D. B. Directed Immobilization of Protein-Coated Nanospheres to Nanometer-Scale Patterns Fabricated by Electron Beam Lithography of Poly(ethylene glycol) Self-Assembled Monolayers. *Langmuir* **2006**, *22*, 5100–5107.

54. Kulakovich, O.; Strekal, N.; Yaroshevich, A.; Maskevich, S.; Gaponenko, S.; Nabiev, I.; Woggon, U.; Artemyev, M. Enhanced Luminescence of CdSe Quantum Dots on Gold Colloids. *Nano Lett,* **2002**, *2*, 1449–1452.

55. Fu, Y.; Lakowicz, J. R. Modification of Single Molecule Fluorescence Near Metallic Nanostructures. *Laser Photonics Rev,* **2009**, *3*, 221–232.

56. Pesen, D.; Haviland, D. B. Modulation of Cell Adhesion Complexes by Surface Protein Patterns. *ACS Appl. Mater. Interfaces* **2009**, *1*, 543–548.

57. Monge, C.; Saha, N.; Boudou, T.; Pozos-Vasquez, C.; Dulong, V.; Glinel, K.; Picart, C. Rigidity-Patterned Polyelectrolyte Films To Control Myoblast Cell Adhesion and Spatial Organization. *Adv. Funct. Mater.* **2013**, 10.1002/adfm.201203580.